Int. J. Appl. Math. Comput. Sci., 2020, Vol. 30, No. 3, 475–491
DOI: 10.34768/amcs-2020-0035

APPROXIMATE STATE–SPACE AND TRANSFER FUNCTION MODELS FOR 2×2 LINEAR HYPERBOLIC SYSTEMS WITH COLLOCATED BOUNDARY INPUTS

KRZYSZTOF BARTECKI [a]

[a] Institute of Control Engineering
Opole University of Technology
ul. Prószkowska 76, 45-758 Opole, Poland
e-mail: K.Bartecki@po.edu.pl

Two approximate representations are proposed for distributed parameter systems described by two linear hyperbolic PDEs with two time- and space-dependent state variables and two collocated boundary inputs. Using the method of lines with the backward difference scheme, the original PDEs are transformed into a set of ODEs and expressed in the form of a finite number of dynamical subsystems (sections). Each section of the approximation model is described by state-space equations with matrix-valued state, input and output operators, or, equivalently, by a rational transfer function matrix. The cascade interconnection of a number of sections results in the overall approximation model expressed in finite-dimensional state-space or rational transfer function domains, respectively. The discussion is illustrated with a practical example of a parallel-flow double-pipe heat exchanger. Its steady-state, frequency and impulse responses obtained from the original infinite-dimensional representation are compared with those resulting from its approximate models of different orders. The results show better approximation quality for the "crossover" input–output channels where the in-domain effects prevail as compared with the "straightforward" channels, where the time-delay phenomena are dominating.

Keywords: distributed parameter system, hyperbolic equations, approximation model, state space, transfer function.

1. Introduction

The analysis of even linear mathematical models of distributed parameter systems (DPSs) can be much more challenging, due to their mathematical complexity, than in the case of lumped parameter systems (LPSs), where the spatial effects are neglected or averaged. Therefore, in practical applications, the original infinite-dimensional models of DPSs are often replaced by their various finite-dimensional approximations. A typical example is the *indirect controller design* (also known as *early lumping*) procedure, where the first step towards the controller design is the finite-dimensional approximation of the original infinite-dimensional model of the system being controlled. Despite some drawbacks, this approach has the advantage of making available a wide range of tools intended for controller design for finite-dimensional systems, assuming that the controller designed using the finite-dimensional approximation has the desired effect on the original system (Ray, 1981; Curtain and Morris, 2009; Li and Qi, 2010; Jones and Kerrigan, 2010; Levine, 2011; Rauh *et al.*, 2016).

Depending on the type of the mathematical representation used to describe the approximation model, different control schemes can be subsequently applied. For example, if a transfer function model is available, it is possible to design a controller using well-known frequency-domain techniques. On the other hand, state-space models allow using various state feedback algorithms, such as, e.g., linear-quadratic (LQR) or linear-quadratic-Gaussian (LQG) control schemes. Finally, for both kinds of the above-mentioned representations, various model predictive control (MPC) strategies can be used.

In the current paper we consider approximate state-space and transfer function models for a certain class of DPSs, the so-called 2×2 hyperbolic systems of balance laws. This class includes phenomena such as those occurring in pipelines, oil wells, irrigation channels, heat exchangers and traffic flow systems, and has recently been intensively studied in the literature (Bastin and

Coron, 2016; Bartecki, 2016; Deutscher, 2017; Anfinsen and Aamo, 2019; Kitsos *et al.*, 2019; Coron *et al.*, 2019), to mention only some recent works.

As shown in some previous works on DPSs, their state-space representation can be made similar to the classical one used for the finite-dimensional systems. However, instead of the state matrix A we have here an unbounded differential state operator acting on a suitable function space. The role of the input and output matrices B and C is played by some control and observation operators, respectively, which are often also unbounded (see, e.g., Curtain and Zwart, 1995; Emirsajłow and Townley, 2000; Arov *et al.*, 2012; Bartecki, 2015a). Also the well-known definition of the transfer function, as the input–output mapping defined in the Laplace transform domain, remains valid for the considered infinite-dimensional case. However, the transfer functions are usually irrational here and contain transcendental and/or fractional functions of the complex variable s. It causes some features which do not appear in the finite-dimensional case, such as an infinite number of poles and/or zeros, and, consequently, infinite "oscillations" in their frequency responses (see, e.g., Callier and Winkin, 1993; Zwart, 2004; Curtain and Morris, 2009; Bartecki, 2013b).

Therefore, a lot of attention has been paid so far to the approximation of various DPS models, also of those described by hyperbolic PDEs resulting from the balance laws of continuum physics. However, the resulting approximations are usually given in the form of numerical models obtained from various conservative finite difference or finite volume schemes (Godlewski and Raviart, 1996; Cockburn *et al.*, 1998; Ahmad and Berzins, 2001; LeVeque, 2002; Shakeri and Dehghan, 2008; Gugat *et al.*, 2018), which are not very convenient for control system design. To the best of the author's knowledge, no, or very little, previous research has regarded approximation models in the form of state-space or transfer function models for 2×2 hyperbolic systems. One of the few is the work of Litrico and Fromion (2009b) where rational transfer function models are used to obtain finite-dimensional approximations for linearized open channel flow equations.

To further reduce the gap, in this paper we propose approximate finite-dimensional state-space and rational transfer function models for the given 2×2 linear hyperbolic systems with a specific, collocated configuration of boundary inputs. It can be seen as a significant extension and continuation of the idea presented for the first time by Bartecki (2019), who proposed an approximate state-space model. The current paper is organized as follows. Section 2 recalls the mathematical model of the considered DPSs in the form of weakly coupled linear hyperbolic PDEs with boundary conditions representing collocated boundary inputs signals. The models in the form of infinite-dimensional state-space equations as well as of irrational transfer functions are recalled, together with the constant steady-state analysis. The relationship of these models to the frequency- and time-domain responses of the system is also reminded here. Section 3 introduces the approximation model based on the *method of lines* (MOL) with the backward difference scheme applied to the spatial domain, giving as a result the high finite-dimensional model in the form of ordinary differential equations (ODEs). Next, the state-space and transfer function representations resulting from the MOL approximation model are derived and their stability analysis is performed. In Section 4 the parallel-flow double-pipe heat exchanger is considered as a typical example of the 2×2 hyperbolic systems with collocated boundary inputs. Its finite-dimensional state-space and transfer function representations are considered for different numbers of spatial sections. The constant steady-state, frequency- and time-domain responses of the original PDE model of the exchanger are compared with those obtained from its approximations of different orders. The model approximation quality is assessed, both by the visual comparison of their frequency- and time-domain responses and the frequency-domain analysis of approximation error magnitudes. The article concludes with Section 5 containing a short summary and directions for further research.

2. 2×2 Linear hyperbolic systems

2.1. PDE representation. We consider dynamical systems which can be mathematically described, usually after some simplifying assumptions, by the following system of the two weakly coupled linear PDEs of hyperbolic type (Bastin and Coron, 2016; Bartecki, 2016; Anfinsen and Aamo, 2018; Kitsos *et al.*, 2019):

$$\frac{\partial x\,(l,t)}{\partial t} + \Lambda \frac{\partial x\,(l,t)}{\partial l} = K x\,(l,t)\,, \tag{1}$$

where

$$x(l,t) = \begin{bmatrix} x_1(l,t) & x_2(l,t) \end{bmatrix}^T : \Omega \times \Theta \to \mathbb{R}^2 \tag{2}$$

is a vector function representing the spatiotemporal distribution of the two state variables, with $\Omega = [0, L]$ being the domain of the one-dimensional spatial variable l and $\Theta = [0, +\infty)$, the domain of the time variable t.

Furthermore, Λ and K in (1) are uniform and time-invariant (i.e., independent of l and t, respectively) matrices of coefficients,

$$\Lambda = \begin{bmatrix} \lambda_1 & 0 \\ 0 & \lambda_2 \end{bmatrix}, \quad K = \begin{bmatrix} k_{11} & k_{12} \\ k_{21} & k_{22} \end{bmatrix}, \tag{3}$$

with $k_{11}, k_{12}, k_{21}, k_{22} \in \mathbb{R}$ representing the so-called *source terms* (i.e., the in-domain coupling coefficients)

and $\lambda_1, \lambda_2 \in \mathbb{R}^+$ being the *characteristic speeds* of the system, usually representing the mass or energy transport rates. In general, λ_1 and λ_2 can be of any sign, but we consider here the specific case of the two mass or energy flows going in the same direction, i.e., from $l = 0$ to $l = L$.

In order to obtain a unique solution of (1), the appropriate *initial* and *boundary* conditions need to be specified. The initial conditions describe the spatial profiles of both state variables at $t = 0$,

$$x_1(l,0) = x_{10}(l), \quad x_2(l,0) = x_{20}(l), \tag{4}$$

where $x_{10}(l), x_{20}(l) : \Omega \to \mathbb{R}$ are functions representing these initial profiles.

Furthermore, the boundary conditions represent the requirements to be met by the solution at the boundary points of Ω, i.e., at $l = 0$ or/and at $l = L$. In general, they can express the boundary reflections and feedbacks (i.e., the interconnections between the state variables at $l = 0$ and/or at $l = L$), as well as they can take into account the *boundary inputs* to the system. The latter case is particularly important in the control problems when the manipulated control inputs are physically located at the system boundaries.

Therefore, in this paper we assume that the boundary conditions are expressed directly by the inhomogeneities introduced by the two external inputs, without any feedback or reflection. Since we take into account the case of $\lambda_1 > 0$ and $\lambda_2 > 0$ in (3), both considered boundary conditions should be imposed at $l = 0$,

$$x_1(0,t) = u_1(t), \quad x_2(0,t) = u_2(t), \tag{5}$$

with $u_1(t)$, $u_2(t) : \Theta \to \mathbb{R}$ being the Laplace transformable input signals which can include both controls and external disturbances (see Bartecki, 2013b).

In addition to the above-mentioned boundary inputs to the system, we also introduce two *output signals*, given as pointwise "observations" or "measurements" of the state variables performed usually at the end of the spatial domain,

$$y_1(t) = x_1(L,t), \quad y_2(t) = x_2(L,t), \tag{6}$$

which may be considered *anti-collocated* to the boundary inputs (5).

We omit here the detailed analysis concerned with the existence and well-posedness of the solutions of the system (1)–(6) since it has been already done, e.g., by Litrico and Fromion (2009a) based on the important results presented by Russell (1978) as well as Curtain and Zwart (1995). These issues have been also thoroughly analyzed for more general classes of hyperbolic systems by Bastin and Coron (2016). As shown there, the exponential convergence of the solution of the Cauchy problem (1)–(4) to zero in the $\mathcal{L}_2$ norm is guaranteed for the matrix $K+K^T$ in (3) being negative-semidefinite, i.e., for

$$\xi^T(K + K^T)\xi \le 0, \quad \forall \xi \in \mathbb{R}^2. \tag{7}$$

It can be understood that the associated physical system has no internal energy sources and only dissipates energy, which is satisfied by many chemical and thermal engineering systems like tubular reactors and heat exchangers.

2.2. State-space representation. The classical state space representation of finite-dimensional linear systems usually includes, except the matrix state operator A, also the input and output operators represented by the matrices B and C, and sometimes also the feedthrough matrix D. For the considered case of infinite-dimensional systems, various abstract state space representations can be used which have been discussed, e.g., by Curtain and Zwart (1995), Emirsajłow and Townley (2000), Grabowski and Callier (2001) or Bartecki (2015a). One of these representations, the so-called *additive form* of the state equations, is based on the same general concept as the one used for the finite-dimensional systems, and for this reason it will be recalled below.

Result 1. *The state and output equations for the system introduced in Section 2.1 can be expressed as follows:*

$$\frac{\mathrm{d}x(t)}{\mathrm{d}t} = Ax(t) + Bu(t), \quad t \ge 0, \quad x(0) = x_0, \tag{8}$$

$$y(t) = Cx(t), \tag{9}$$

where $x(t)$ represents the state variables in (2) defined on the following Hilbert function space $\mathcal{X}$

$$x(t) = \begin{bmatrix} x_1(t) & x_2(t) \end{bmatrix}^T \in \mathcal{X} = \mathcal{L}^2(\Omega, \mathbb{R}) \oplus \mathcal{L}^2(\Omega, \mathbb{R}), \tag{10}$$

$u(t)$ is the vector of boundary input signals in (5)

$$u(t) = \begin{bmatrix} u_1(t) & u_2(t) \end{bmatrix}^T \in \mathbb{R}^2, \tag{11}$$

$y(t)$ is the vector of output signals in (6)

$$y(t) = \begin{bmatrix} y_1(t) & y_2(t) \end{bmatrix}^T \in \mathbb{R}^2, \tag{12}$$

$A : \mathcal{X} \supset D(A) \to \mathcal{X}$ is the differential state operator *based on (1) and given by*

$$Ah = -\Lambda \frac{\mathrm{d}h}{\mathrm{d}l} + Kh, \quad h = [h_1, h_2]^T \in D(A), \tag{13}$$

with the following domain:

$$D(A) = \big\{ \{h \in \mathcal{H}^1(\Omega, \mathbb{R}) \oplus \mathcal{H}^1(\Omega, \mathbb{R})\} \big| \; h_1(0) = h_2(0) = 0 \big\}, \tag{14}$$

where $\mathcal{H}^1(\Omega,\mathbb{R})$ is the Sobolev space of functions with first distributional derivatives lying in $\mathcal{L}^2(\Omega,\mathbb{R})$.

B in (8) represents an unbounded boundary input operator *which for the considered collocated input configuration (5) takes the following form:*

$$B = \operatorname{diag}\left(\lambda_1\delta(l), \lambda_2\delta(l)\right), \tag{15}$$

where $\delta(l)$, $l \in \Omega$, denotes the Dirac delta distribution.

Finally, C in (9) is the following output operator

$$Cx(t) = \begin{bmatrix} \int_0^L \delta(\mu - L)x_1(\mu,t)\mathrm{d}\mu \\ \int_0^L \delta(\mu - L)x_2(\mu,t)\mathrm{d}\mu \end{bmatrix} = \begin{bmatrix} x_1(L,t) \\ x_2(L,t) \end{bmatrix}, \tag{16}$$

which results from (6) and is based on the so-called sifting property of the Dirac delta distribution.

Proof. See the work of Bartecki (2015a). ■

Remark 1. The most important consequence of the form of the boundary input operator (15) is that the state equation (8) should be studied in an extrapolation space $\mathcal{X}_{-1}$, which is a completion of $\mathcal{X}$ in (10) with an A-resolvent-induced norm (Engel and Nagel, 2000; Tucsnak and Weiss, 2009). Therefore, the presented form of the state-space equations, although at first glance seems to be attractive because it resembles a classic finite-dimensional concept, may not be very convenient for control engineers.

2.3. Transfer function representation. In contrast to the lumped parameter systems which are described by the rational transfer functions, the transfer functions of distributed parameter systems are irrational (e.g., Zwart, 2004; Curtain and Morris, 2009). Transfer function analysis of the considered hyperbolic systems of balance laws was the subject of some of the author's papers (see, e.g., Bartecki, 2013a), as well as his monograph (Bartecki, 2016). Therefore, the results relating to the irrational transfer function representation of the 2×2 hyperbolic systems with collocated boundary inputs are recalled below.

Result 2. *Assuming that the observation (measurement) of both state variables x_1 and x_2 in (2) can be made at any spatial point $l \in \Omega$, we introduce the following* distributed transfer function *matrix $G(l,s)$:*

$$G(l,s) = \begin{bmatrix} g_{11}(l,s) & g_{12}(l,s) \\ g_{21}(l,s) & g_{22}(l,s) \end{bmatrix}, \tag{17}$$

where

$$g_{11}(l,s) = \frac{x_1(l,s)}{u_1(s)}, \quad g_{12}(l,s) = \frac{x_1(l,s)}{u_2(s)}, \tag{18}$$

$$g_{21}(l,s) = \frac{x_2(l,s)}{u_1(s)}, \quad g_{22}(l,s) = \frac{x_2(l,s)}{u_2(s)}, \tag{19}$$

for zero initial conditions (4), with $x_1(l,s)$, $x_2(l,s)$ and $u_1(s)$, $u_2(s)$ being the Laplace transforms in time of the state (2) and the input (5) variables, respectively[1].

The expressions for the elements of the transfer function matrix $G(l,s)$ in (17) take the following form:

$$\begin{aligned} g_{11}(l,s) &= \frac{\phi_1(s) - p_{22}(s)}{\phi_1(s) - \phi_2(s)} \mathrm{e}^{\phi_1(s)l} \\ &\quad - \frac{\phi_2(s) - p_{22}(s)}{\phi_1(s) - \phi_2(s)} \mathrm{e}^{\phi_2(s)l}, \end{aligned} \tag{20}$$

$$g_{12}(l,s) = \frac{p_{12}}{\phi_1(s) - \phi_2(s)} \left(\mathrm{e}^{\phi_1(s)l} - \mathrm{e}^{\phi_2(s)l}\right), \tag{21}$$

$$g_{21}(l,s) = \frac{p_{21}}{\phi_1(s) - \phi_2(s)} \left(\mathrm{e}^{\phi_1(s)l} - \mathrm{e}^{\phi_2(s)l}\right), \tag{22}$$

$$\begin{aligned} g_{22}(l,s) &= \frac{\phi_1(s) - p_{11}(s)}{\phi_1(s) - \phi_2(s)} \mathrm{e}^{\phi_1(s)l} \\ &\quad - \frac{\phi_2(s) - p_{11}(s)}{\phi_1(s) - \phi_2(s)} \mathrm{e}^{\phi_2(s)l}, \end{aligned} \tag{23}$$

where

$$p_{11}(s) = \frac{k_{11} - s}{\lambda_1}, \qquad p_{12} = \frac{k_{12}}{\lambda_1}, \tag{24}$$

$$p_{21} = \frac{k_{21}}{\lambda_2}, \qquad p_{22}(s) = \frac{k_{22} - s}{\lambda_2}. \tag{25}$$

and

$$\phi_{1,2}(s) = \alpha(s) \pm \beta(s), \tag{26}$$

with

$$\alpha(s) = \frac{1}{2}\left(p_{11}(s) + p_{22}(s)\right), \tag{27}$$

$$\beta(s) = \frac{1}{2}\sqrt{\left(p_{11}(s) - p_{22}(s)\right)^2 + 4p_{12}p_{21}}. \tag{28}$$

Proof. It proceeds by using the Laplace transform method; for details, see the work of Bartecki (2013b). ■

Corollary 1. *Assuming that the observation (measurement) of both state variables x_1 and x_2 is performed at the boundary outputs y_1 and y_2 given by (6), we obtain, based on Result 2, the following* boundary transfer function *matrix $G(s) = G(L,s)$:*

$$G(s) = \begin{bmatrix} g_{11}(s) & g_{12}(s) \\ g_{21}(s) & g_{22}(s) \end{bmatrix}, \tag{29}$$

where

$$g_{11}(s) = \frac{y_1(s)}{u_1(s)}, \quad g_{12}(s) = \frac{y_1(s)}{u_2(s)}, \tag{30}$$

$$g_{21}(s) = \frac{y_2(s)}{u_1(s)}, \quad g_{22}(s) = \frac{y_2(s)}{u_2(s)}, \tag{31}$$

[1] We stick to the notation $x(l,s)$ and $u(s)$ assuming that the parameter s alone indicates the Laplace transform in time of $x(l,t)$ and $u(t)$, respectively.

with the expressions for the transfer functions (30)–(31) obtained by substituting $l = L$ in (20)–(23).

Corollary 2. *From Result 2 we have that the vector of the Laplace-transformed state variables (2) can be obtained, assuming zero initial conditions, from the following relationship:*

$$x(l,s) = G(l,s)u(s), \tag{32}$$

with $u(s)$ being the Laplace transformed boundary input vector (11). Similarly, we can obtain the vector of the Laplace-transformed output signals (12) as

$$y(s) = G(s)u(s), \tag{33}$$

where $G(s)$ is the boundary transfer function matrix given by Corollary 1.

Remark 2. It can be shown that the transfer function matrix $G(s)$ given by Corollary 1 belongs to the *Hardy space* $\mathcal{H}_\infty^{2,2}$, defined as the space of functions $G : \mathbb{C} \to \mathbb{C}^{2,2}$ which are analytic and bounded in the open right half of the complex plane, $\mathrm{Re(s)} > 0$ (see Callier and Winkin, 1993). Moreover, as can be seen from (24)–(28), these transfer functions have fractional powers of s. Therefore, they can also be classified as *fractional transfer functions* which have been receiving increasing attention in the literature (see Curtain and Morris, 2009).

2.4. Constant steady-state solution. In the case of DPSs, the steady-state solution provides not only information about the static input–output mappings as it does for LPSs, but it also describes the fixed distribution of the state variables inside the spatial domain of the system. Below, the definition of the constant steady-state solution is formulated and next, the expressions for the steady-state distribution of the state variables are shown for the considered 2×2 hyperbolic systems.

Definition 1. The constant steady-state solution

$$\bar{x}(l) = \begin{bmatrix} \bar{x}_1(l) & \bar{x}_2(l) \end{bmatrix}^T : \Omega \to \mathbb{R}^2 \tag{34}$$

of the initial-boundary value problem (1)–(5) is a solution that does not depend on time, i.e., the one which can be obtained by the assumption that the time derivative in (1) is zero,

$$\frac{\partial x_1(l,t)}{\partial t} = \frac{\partial x_2(l,t)}{\partial t} = 0, \tag{35}$$

which defines an equilibrium point of the system, together with the assumption on constant boundary conditions (5)

$$\bar{x}_1(0) = \bar{u}_1, \quad \bar{x}_2(0) = \bar{u}_2, \quad \bar{u}_1, \bar{u}_2 \in \mathbb{R}. \tag{36}$$

Result 3. *The constant steady-state spatial distribution of the state variables x_1 and x_2 of the system (1)–(5) can be expressed, assuming constant collocated boundary inputs (36), by the following equations:*

$$\begin{aligned} \bar{x}_1(l) = &\left(\frac{\lambda_2\phi_1 - k_{22}}{2\lambda_2\beta} \mathrm{e}^{\phi_1 l} - \frac{\lambda_2\phi_2 - k_{22}}{2\lambda_2\beta} \mathrm{e}^{\phi_2 l} \right) \bar{u}_1 \\ &+ \frac{k_{12}}{2\lambda_1\beta} \left(\mathrm{e}^{\phi_1 l} - \mathrm{e}^{\phi_2 l} \right) \bar{u}_2, \end{aligned} \tag{37}$$

$$\begin{aligned} \bar{x}_2(l) = &\frac{k_{21}}{2\lambda_2\beta} \left(\mathrm{e}^{\phi_1 l} - \mathrm{e}^{\phi_2 l} \right) \bar{u}_1 \\ &+ \left(\frac{\lambda_1\phi_1 - k_{11}}{2\lambda_1\beta} \mathrm{e}^{\phi_1 l} - \frac{\lambda_1\phi_2 - k_{11}}{2\lambda_1\beta} \mathrm{e}^{\phi_2 l} \right) \bar{u}_2, \end{aligned} \tag{38}$$

where $\phi_{1,2} = \phi_{1,2}(0)$, $\alpha = \alpha(0)$ and $\beta = \beta(0)$ are given by (26), (27) and (28), respectively, assuming $s = 0$.

Proof. After setting to zero the time derivative in (1) and replacing $x(l,t)$ by $\bar{x}(l)$, we obtain the following system of two ODEs:

$$\lambda_1 \frac{\mathrm{d}\bar{x}_1(l)}{\mathrm{d}l} = k_{11}\bar{x}_1(l) + k_{12}\bar{x}_2(l), \tag{39}$$

$$\lambda_2 \frac{\mathrm{d}\bar{x}_2(l)}{\mathrm{d}l} = k_{21}\bar{x}_1(l) + k_{22}\bar{x}_2(l), \tag{40}$$

with the boundary conditions (36). The solution of (39) and (40) is then given by (37) and (38). ■

Corollary 3. *The constant steady-state solution $\bar{x}(l)$ given by Result 3 can be alternatively obtained from the relationship*

$$\bar{x}(l) = G(l,0)\bar{u}, \tag{41}$$

where

$$\bar{u} = \begin{bmatrix} \bar{u}_1 & \bar{u}_2 \end{bmatrix}^T \tag{42}$$

is the vector of constant boundary inputs (36) and $G(l,0)$ is the distributed transfer function matrix given by Result 2, evaluated at $s = 0$. Therefore, $G(l,0)$ can be seen as the spatially distributed steady-state gain matrix of the system.

Consequently, the values of the output vector (12) in the constant steady-state conditions can be calculated as

$$\bar{y} = G(0)\bar{u}, \tag{43}$$

where $G(0)$ is the boundary transfer function matrix given by Corollary 1, evaluated at $s = 0$. Therefore, $G(0)$ can be seen as the steady-state boundary gain matrix of the system.

2.5. Frequency- and time-domain responses. In order to obtain frequency responses for the considered systems, we need to replace the operator variable s in the transfer functions given by Result 2 and Corollary 1 with the expression $i\omega$, where $\omega \geq 0$ is the angular frequency. This operation transforms the system representation from the Laplace transform domain to the

Fourier transform domain which, in turn, can be seen as the frequency-domain description of the system. Like in the case of LPSs, the frequency responses can be represented here in a number of ways, of which two are most commonly used: Nyquist and Bode plots.

On the other hand, the time-domain analysis is also possible using the transfer function representation, bearing in mind that it directly expresses Laplace-transformed impulse responses of the system. Therefore, the spatially distributed impulse responses $g_{ij}(l,t)$ can be calculated based on the following formula expressing the inverse Laplace transform:

$$\begin{aligned} g_{ij}(l,t) &= \mathscr{L}_s^{-1}\{g_{ij}(l,s)\} \\ &= \frac{1}{2\pi i}\lim_{T\to\infty}\int_{\alpha-iT}^{\alpha+iT} \mathrm{e}^{st} g_{ij}(l,s)\,\mathrm{d}s, \end{aligned} \tag{44}$$

where $g_{ij}(l,s)$ for $i = 1,2$ and $j = 1,2$ represent the distributed transfer functions given by Result 2. By replacing the distributed transfer function $g_{ij}(l,s)$ in (44) by its boundary counterpart $g_{ij}(s) = g_{ij}(L,s)$ given by Corollary 1, we obtain as a result the boundary impulse response $g_{ij}(t)$, i.e., the impulse response evaluated at $l = L$. The calculations of the Bromwich integral in (44) along the vertical line $\mathrm{Re}(s) = \alpha$ can be facilitated, e.g., by the use of the Cauchy residue theorem. For practical reasons, this laborious task can be replaced by finding the expressions for the inverse Laplace transforms in look-up tables (see, e.g., Polyanin and Manzhirov, 1998). The analytical formulas for the impulse responses of the considered hyperbolic systems can be found in the monograph by Bartecki (2016).

3. Approximation models

This section deals with the finite-dimensional approximation models of the considered 2×2 hyperbolic systems with collocated boundary inputs, introduced in Section 2. In Section 3.1, by using the method of lines we replace the original PDE representation of the system by a set of ODEs. Next, based on the ODE representation, the finite-dimensional state-space approximation model is derived in Section 3.2. In a similar way, the rational transfer function approximation model is developed in Section 3.3. Finally, Section 3.4 deals with the frequency- and time-domain measures of the approximation error.

3.1. MOL approximation. The idea of the method of lines (MOL) consists in replacing the spatial derivatives in a PDE with their algebraic approximations. This can be done using several methods, such as, e.g., finite elements, splines, weighted residuals or polynomial approximations. Once this is done, the spatial derivatives are no longer stated in terms of the spatial independent variables. In effect, only the time variable remains in the resulting equations (Ahmad and Berzins, 2001; Koto, 2004; Schiesser and Griffiths, 2009). The most important advantage of the MOL approach is that it has not only the simplicity of the explicit methods, but also the stability advantage of the implicit ones unless a poor numerical method for solution of ODEs is employed. It is possible to achieve higher-order approximations in the discretization of spatial derivatives without significant increases in the computational complexity (Shakeri and Dehghan, 2008).

In order to obtain the approximation model for the hyperbolic system introduced in Section 2.1, we use the finite difference (FD) method. For the assumed case of both positive characteristic speeds $\lambda_1 > 0$ and $\lambda_2 > 0$, the *backward difference* is applied, which results in replacing the spatial derivatives in (1) with their algebraic approximations (Mattheij *et al.*, 2005):

$$\frac{\partial x_1(l,t)}{\partial l} \approx \frac{x_{1,n}(t) - x_{1,n-1}(t)}{\Delta l_n}, \tag{45}$$

$$\frac{\partial x_2(l,t)}{\partial l} \approx \frac{x_{2,n}(t) - x_{2,n-1}(t)}{\Delta l_n}, \tag{46}$$

where

$$x_{1,n}(t) = x_1(l_n,t), \quad x_{2,n}(t) = x_2(l_n,t), \tag{47}$$

represent the values of the state variables at the spatial discretization points l_n, $n = 1,2,\ldots,N$, assuming that $l_0 = 0$, $l_N = L$, and

$$\Delta l_n = l_n - l_{n-1} \tag{48}$$

is the spatial grid size, which, in general, does not have to be the same for different n.

As a result, the approximation model takes here the form of a system of $2N$ ODEs, with the following two equations representing the single n-th section:

$$\begin{aligned} \frac{\mathrm{d}x_{1,n}(t)}{\mathrm{d}t} =& -\frac{\lambda_1}{\Delta l_n}x_{1,n}(t) + \frac{\lambda_1}{\Delta l_n}x_{1,n-1}(t) \\ &+ k_{11}x_{1,n}(t) + k_{12}x_{2,n}(t), \end{aligned} \tag{49}$$

$$\begin{aligned} \frac{\mathrm{d}x_{2,n}(t)}{\mathrm{d}t} =& -\frac{\lambda_2}{\Delta l_n}x_{2,n}(t) + \frac{\lambda_2}{\Delta l_n}x_{2,n-1}(t) \\ &+ k_{21}x_{1,n}(t) + k_{22}x_{2,n}(t), \end{aligned} \tag{50}$$

where $x_{1,n-1}(t)$ and $x_{2,n-1}(t)$ can be considered as two section inputs, whereas $x_{1,n}(t)$ and $x_{2,n}(t)$ can be taken as two section outputs.

The considered ODE approximation model can be therefore seen as a cascade interconnection of N sections, each given by (49)–(50), with the section outputs being connected to the corresponding inputs of the next section. In addition, we notice that the inputs to the first section should be identified with the system boundary inputs (5),

whereas the outputs of the last (N-th) section represent approximate system outputs (6).

Finally, the initial conditions (4) are transformed here to the following form:

$$x_{1,n}(0) = x_{10,n} = x_{10}(l_n), \tag{51}$$
$$x_{2,n}(0) = x_{20,n} = x_{20}(l_n), \tag{52}$$

where $x_{10}(l_n)$ and $x_{20}(l_n)$ are the initial profile values of both state variables in (4) evaluated at $l = l_n$.

3.2. State-space representation. In the following three paragraphs, the state-space representation of the considered approximation model is discussed, for both the single section and the resultant N-section model.

3.2.1. Single section. Introduce the following output/state vector for the n-th section of the MOL approximation model discussed in Section 3.1:

$$\begin{aligned} y_{(n)}(t) &= \begin{bmatrix} y_{1,n}(t) & y_{2,n}(t) \end{bmatrix}^T \\ &= x_{(n)}(t) = \begin{bmatrix} x_{1,n}(t) & x_{2,n}(t) \end{bmatrix}^T \end{aligned} \tag{53}$$

together with the section input vector given for $n = 2, 3, \ldots, N$ by

$$\begin{aligned} u_{(n)}(t) &= \begin{bmatrix} u_{1,n}(t) & u_{2,n}(t) \end{bmatrix}^T \\ &= x_{(n-1)}(t) = \begin{bmatrix} x_{1,n-1}(t) & x_{2,n-1}(t) \end{bmatrix}^T, \end{aligned} \tag{54}$$

and for $n = 1$ by the boundary input signals (5). As can be seen, the output signals of the n-th section, $n = 1, 2, \ldots, N-1$, are considered to be the input signals for the next $(n+1)$-th section, which corresponds to the cascade interconnection of the individual sections.

Result 4. *The state-space equations of the single n-th section of the approximation model take the following form:*

$$\frac{\mathrm{d}x_{(n)}(t)}{\mathrm{d}t} = A_n x_{(n)}(t) + B_n u_{(n)}(t)\,, \tag{55}$$
$$y_{(n)}(t) = C_n x_{(n)}(t)\,, \tag{56}$$

where

$$A_n = \begin{bmatrix} -\frac{\lambda_1}{\Delta l_n} + k_{11} & k_{12} \\ k_{21} & -\frac{\lambda_2}{\Delta l_n} + k_{22} \end{bmatrix}, \tag{57}$$

$$B_n = \begin{bmatrix} \frac{\lambda_1}{\Delta l_n} & 0 \\ 0 & \frac{\lambda_2}{\Delta l_n} \end{bmatrix}, \quad C_n = \begin{bmatrix} 1 & 0 \\ 0 & 1 \end{bmatrix}, \tag{58}$$

are the state, input and output matrices of the n-th section, respectively. The state equation (55) is completed by the initial conditions (51)–(52).

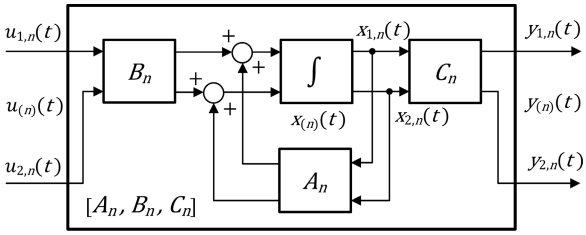

Fig. 1. Single section of the approximate state-space model.

Proof. It is based on (49)–(50) and (53)–(54). ■

The structure of the single section of the approximate state-space model is presented in Fig. 1.

As it can be easily shown, the characteristic polynomial of the state matrix A_n in (57) is given by

$$p_{A_n}(s) = \det(sI - A_n) = s^2 + a_{1,n}s + a_{0,n} \tag{59}$$

with

$$a_{1,n} = \frac{\lambda_1}{\Delta l_n} + \frac{\lambda_2}{\Delta l_n} - k_{11} - k_{22}, \tag{60}$$
$$a_{0,n} = \left(k_{11} - \frac{\lambda_1}{\Delta l_n}\right)\left(k_{22} - \frac{\lambda_2}{\Delta l_n}\right) - k_{21}k_{12}. \tag{61}$$

In order to ensure the asymptotic stability of the section, both eigenvalues of A_n in (57) which are given by

$$s_{(1,2),n} = -\frac{a_{1,n}}{2} \pm \frac{\sqrt{a_{1,n}^2 - 4a_{0,n}}}{2}, \tag{62}$$

need to have negative real parts, i.e.,

$$\mathrm{Re}\left\{s_{(1,2),n}\right\} < 0, \tag{63}$$

which will be satisfied, e.g., for A_n being diagonally dominant with negative diagonal elements. A more detailed result is given below.

Result 5. *The eigenvalues (62) of the state matrix A_n in (57) are real for $a_{1,n}^2 \geq 4a_{0,n}$ and complex for $a_{1,n}^2 < 4a_{0,n}$. In the second case, the complex conjugate pair is asymptotically stable for $a_{1,n} > 0$, which can be written, based on (60), as*

$$\frac{\lambda_1 + \lambda_2}{\Delta l_n} > k_{11} + k_{22}, \tag{64}$$

which means that Δl_n needs to be sufficiently small compared with the characteristic speeds λ_1, λ_2 and source terms k_{11}, k_{22}.

For the case of real eigenvalues, the asymptotic stability condition (64) needs to be complemented by the additional requirement $a_{0,n} > 0$, which can be written based on (61) as

$$\left(k_{11} - \frac{\lambda_1}{\Delta l_n}\right)\left(k_{22} - \frac{\lambda_2}{\Delta l_n}\right) > k_{12} + k_{21}. \tag{65}$$

Proof. It results directly from (59)–(63). ■

Remark 3. As can be seen from (55)–(58), the matrices A_n, B_n and C_n represent a controllable and observable dynamical subsystem (see also Fig. 1).

3.2.2. N-section model. Introduce the following state vector $\hat{x}(t)$ of the approximation model consisting of N cascade interconnected sections discussed in Paragraph 3.2.1 (see also Fig. 3 later in the paper):

$$\begin{aligned}\hat{x}(t) &= \left[x_{(1)}(t) \dots\ x_{(N)}(t)\right]^T \\ &= \left[x_{1,1}(t) \quad x_{2,1}(t)\ \dots\ x_{1,N}(t) \quad x_{2,N}(t)\right]^T,\end{aligned} \tag{66}$$

together with the boundary input vector $u(t)$ in (11) affecting its first section ($n = 1$)

$$u(t) = u_{(1)}(t) = \left[u_{1,1}(t) \quad u_{2,1}(t)\right]^T, \tag{67}$$

and the approximated output vector $\hat{y}(t)$ in (12) taken from the last section ($n = N$)

$$\hat{y}(t) = y_{(N)}(t) = \left[y_{1,N}(t) \quad y_{2,N}(t)\right]^T. \tag{68}$$

Result 6. *The state-space representation of the overall N-section approximation model takes the following form:*

$$\frac{\mathrm{d}\hat{x}(t)}{\mathrm{d}t} = \hat{A}\hat{x}(t) + \hat{B}u(t), \tag{69}$$

$$\hat{y}(t) = \hat{C}\hat{x}(t), \tag{70}$$

where $\hat{A} \in \mathbb{R}^{2N\times 2N}$, $\hat{B} \in \mathbb{R}^{2N\times 2}$ and $\hat{C} \in \mathbb{R}^{2\times 2N}$ are approximated state, input and output operators, respectively, given by the following matrices:

$$\hat{A} = \begin{bmatrix} A_1 & 0_{2\times2} & 0_{2\times2} & 0_{2\times2} & \cdots & \cdots & 0_{2\times2} \\ B_2C_1 & A_2 & 0_{2\times2} & 0_{2\times2} & \cdots & \cdots & 0_{2\times2} \\ 0_{2\times2} & B_3C_2 & A_3 & 0_{2\times2} & \cdots & \cdots & 0_{2\times2} \\ 0_{2\times2} & 0_{2\times2} & B_4C_3 & \ddots & \ddots & \cdots & 0_{2\times2} \\ 0_{2\times2} & 0_{2\times2} & 0_{2\times2} & \ddots & \ddots & \ddots & \vdots \\ \vdots & \vdots & \vdots & \ddots & \ddots & A_{N-1} & 0_{2\times2} \\ 0_{2\times2} & 0_{2\times2} & 0_{2\times2} & \cdots & 0_{2\times2} & B_NC_{N-1} & A_N \end{bmatrix}, \tag{71}$$

$$\hat{B} = \left[B_1 \quad 0_{2\times2} \quad \cdots \quad 0_{2\times2}\right]^T, \tag{72}$$

$$\hat{C} = \left[0_{2\times2} \quad \cdots \quad 0_{2\times2} \quad C_N\right], \tag{73}$$

where A_n, B_n, C_n, for $n = 1, 2, \dots, N$, are the state, input and output matrices of the individual sections given by (57) and (58). The state equation (69) is complemented with the initial conditions (51)–(52) for each section of the model.

Proof. It follows directly from the state-space representation of the cascade interconnection of N dynamical subsystems given by the matrices A_n, B_n, C_n (see, e.g., Albertos and Sala, 2004). ■

Corollary 4. *Based on the state equation (69) of Result 6 we have that the Laplace-transformed approximate state vector (66) can be obtained, assuming zero initial conditions, from the relationship*

$$\hat{x}(s) = \left(sI - \hat{A}\right)^{-1}\hat{B}u(s), \quad s \in \rho(\hat{A}), \tag{74}$$

where $\hat{A}$ and $\hat{B}$ are the state (71) and input (72) matrices of the approximation model, respectively, $u(s)$ is the Laplace-transformed input vector (67) and $\rho(\hat{A})$ denotes the resolvent set of $\hat{A}$. Taking into account also the output equation (70), we obtain

$$\hat{y}(s) = \hat{C}\left(sI - \hat{A}\right)^{-1}\hat{B}u(s), \quad s \in \rho(\hat{A}), \tag{75}$$

where $\hat{C}$ is the output matrix (73).

Corollary 5. *Based on the properties of the above-mentioned cascade interconnection, it can be stated that the eigenvalues of the state matrix $\hat{A}$ in (71) are given by the union of the eigenvalues of individual sections,*

$$s_{(1,2,\dots,2N-1,2N)} = \bigcup_{n=1}^{N} s_{(1,2),n}. \tag{76}$$

Therefore, in order to ensure the asymptotic stability of the approximate state-space model given by Result 6, all the eigenvalues of the section state matrices A_n, $n = 1, 2, \dots, N$, need to have negative real parts—see Result 5.

Corollary 6. *The approximation of the constant steady-state solutions $\bar{x}(l)$ and $\bar{y}$ given by Result 3 and Corollary 3 can be expressed, using the approximate state-space model from Result 6 and Corollary 4, in the following form:*

$$\bar{\hat{x}} = -\hat{A}^{-1}\hat{B}\bar{u}, \quad \det(\hat{A}) \neq 0, \tag{77}$$

$$\bar{\hat{y}} = \hat{C}\bar{\hat{x}} = -\hat{C}\hat{A}^{-1}\hat{B}\bar{u}, \tag{78}$$

where $\bar{u}$ is the vector of constant boundary input signals (42), $\bar{\hat{x}}$ is the constant steady-state state vector (66) of the approximation model and $\bar{\hat{y}}$ is its constant steady-state output vector (68).

3.3. Transfer function representation. In the following three sections, the transfer function representation for the considered MOL-based approximation model is discussed, starting with the single n-th section and ending with the resultant N-section model.

3.3.1. Single section.

Result 7. *The transfer function matrix $G_n(s)$ of the single n-th section of the approximation model introduced in Section 3.1 takes the following form:*

$$G_n(s) = \begin{bmatrix} g_{11,n}(s) & g_{12,n}(s) \\ g_{21,n}(s) & g_{22,n}(s) \end{bmatrix}, \tag{79}$$

where

$$g_{11,n}(s) = \frac{y_{1,n}(s)}{u_{1,n}(s)}, \quad g_{12,n}(s) = \frac{y_{1,n}(s)}{u_{2,n}(s)}, \tag{80}$$

$$g_{21,n}(s) = \frac{y_{2,n}(s)}{u_{1,n}(s)}, \quad g_{22,n}(s) = \frac{y_{2,n}(s)}{u_{2,n}(s)}, \tag{81}$$

for zero initial conditions (51)-(52), with $y_{1,n}(s)$, $y_{2,n}(s)$ and $u_{1,n}(s)$, $u_{2,n}(s)$ being the Laplace-transformed output and input signals of the n-th section, given by (53) and (54), respectively.

The elements of the transfer function matrix $G_n(s)$ in (79)–(81) take the following form:

$$g_{11,n}(s) = \frac{b_{11,1,n}s + b_{11,0,n}}{s^2 + a_{1,n}s + a_{0,n}}, \tag{82}$$

$$g_{12,n}(s) = \frac{b_{12,0,n}}{s^2 + a_{1,n}s + a_{0,n}}, \tag{83}$$

$$g_{21,n}(s) = \frac{b_{21,0,n}}{s^2 + a_{1,n}s + a_{0,n}}, \tag{84}$$

$$g_{22,n}(s) = \frac{b_{22,1,n}s + b_{22,0,n}}{s^2 + a_{1,n}s + a_{0,n}}, \tag{85}$$

where

$$b_{11,1,n} = \frac{\lambda_1}{\Delta l_n}, \quad b_{11,0,n} = \frac{\lambda_1}{\Delta l_n}\left(\frac{\lambda_2}{\Delta l_n} - k_{22}\right), \tag{86}$$

$$b_{12,0,n} = k_{12}\frac{\lambda_2}{\Delta l_n}, \quad b_{21,0,n} = k_{21}\frac{\lambda_1}{\Delta l_n}, \tag{87}$$

$$b_{22,1,n} = \frac{\lambda_2}{\Delta l_n}, \quad b_{22,0,n} = \frac{\lambda_2}{\Delta l_n}\left(\frac{\lambda_1}{\Delta l_n} - k_{11}\right), \tag{88}$$

and $a_{1,n}$, $a_{0,n}$ are the parameters of the characteristic polynomial given by (59)–(61).

Proof. By applying the Laplace transform to (49) and (50) with zero initial conditions (51) and (52) and solving the resulting equations with respect to $x_{1,n}(s)$ and $x_{2,n}(s)$, we obtain the transfer functions given by (82)–(88). ∎

Remark 4. According to Remark 3, the single section represents a controllable and observable dynamical system, and thus the poles of the transfer functions (82)–(85) are equal to the eigenvalues (62) of the state matrix A_n (57). Therefore, Result 5 concerning stability analysis in terms of the eigenvalues of A_n, remains valid in terms of the poles of $G_n(s)$.

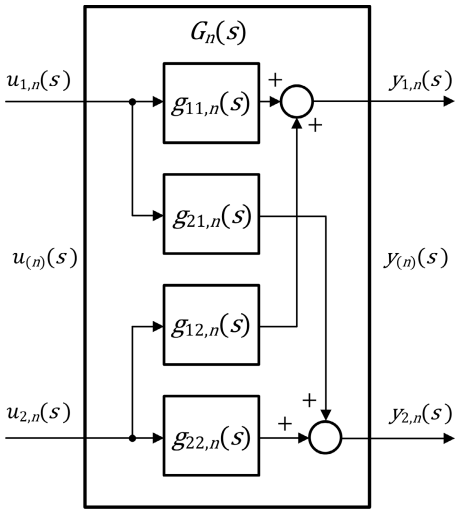

Fig. 2. Single section of the approximate transfer function model.

Corollary 7. *As can be seen from (82)–(85), the relative degree of $g_{11,n}(s)$ and $g_{22,n}(s)$ is equal to 1 and of $g_{12,n}(s)$ and $g_{21,n}(s)$ is equal to 2. In addition, we can state that transfer functions $g_{12,n}(s)$ and $g_{21,n}(s)$ do not have zeros, whereas $g_{11,n}(s)$ and $g_{22,n}(s)$ have single zeros at*

$$z_{11,n} = -\frac{b_{11,0,n}}{b_{11,1,n}} = k_{22} - \frac{\lambda_2}{\Delta l_n}, \tag{89}$$

$$z_{22,n} = -\frac{b_{22,0,n}}{b_{22,1,n}} = k_{11} - \frac{\lambda_1}{\Delta l_n}. \tag{90}$$

Therefore, in order to ensure the minimum-phase property for the single section, the following two conditions should be met simultaneously:

$$\frac{\lambda_1}{\Delta l_n} > k_{11}, \quad \frac{\lambda_2}{\Delta l_n} > k_{22}, \tag{91}$$

which means that the section length should be small enough compared with the system parameters—see the stability condition (64).

The structure of the single section of the approximate transfer function model is presented in Fig. 2.

3.3.2. N-section model.

Consider the approximation model in the form of a cascade interconnection of N sections, each described by the transfer function matrix $G_n(s)$ given by Result 7 (see Fig. 3).

Result 8. *Assuming that the observation of the state variables $x_{1,n}$ and $x_{2,n}$ of the approximation model can be made for any spatial discretization point l_n, $n = 1, 2, \ldots, N$ (i.e., at each section output $y_{1,n}$ and $y_{2,n}$ of*

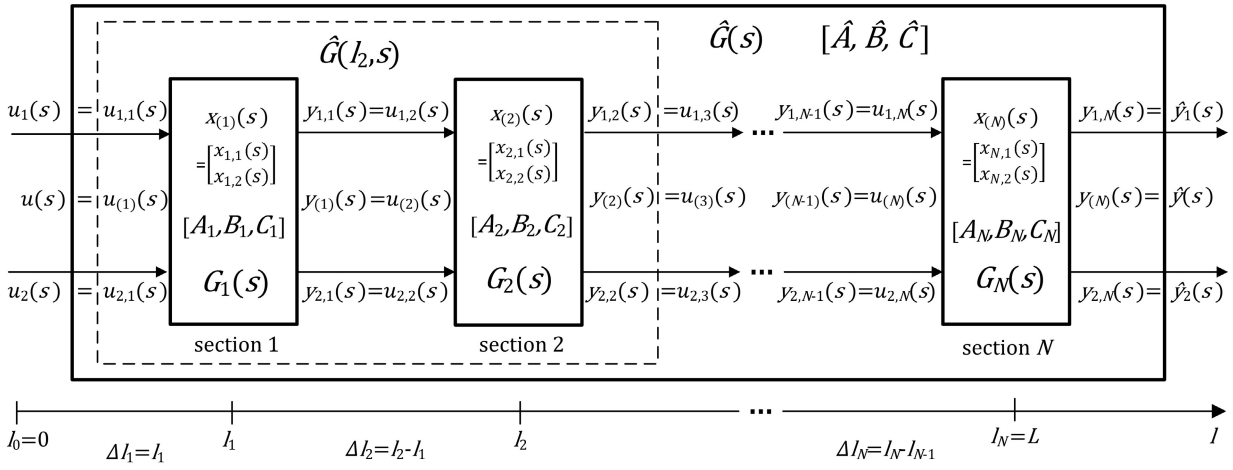

Fig. 3. Block diagram of the approximation state space and transfer function models.

the cascade interconnected model), we introduce the following approximate distributed transfer function *matrix* $\hat{G}(l_n, s)$*:*

$$\hat{G}(l_n,s)=\begin{bmatrix}\hat{g}_{11}(l_n,s) & \hat{g}_{12}(l_n,s)\\ \hat{g}_{21}(l_n,s) & \hat{g}_{22}(l_n,s)\end{bmatrix}, \qquad (92)$$

where

$$\hat{g}_{11}(l_n,s)=\frac{y_{1,n}(s)}{u_1(s)}, \quad \hat{g}_{12}(l_n,s)=\frac{y_{1,n}(s)}{u_2(s)}, \qquad (93)$$

$$\hat{g}_{21}(l_n,s)=\frac{y_{2,n}(s)}{u_1(s)}, \quad \hat{g}_{22}(l,s)=\frac{y_{2,n}(s)}{u_2(s)}, \qquad (94)$$

for zero initial conditions (51)–(52), with $y_{1,n}(s)$*,* $y_{2,n}(s)$ *and* $u_1(s)$*,* $u_2(s)$ *being the Laplace-transformed* n*-th section output (53) and boundary input (67) signals, respectively.*

The transfer function matrix $\hat{G}(l_n, s)$ *given by (92)–(94) can be seen as a rational approximation of the irrational distributed transfer function matrix* $G(l, s)$ *introduced by Result 2 assuming* $l = l_n$*, and it can be calculated as follows:*

$$\hat{G}(l_n,s)=G_n(s)G_{n-1}(s)\dots G_1(s), \qquad (95)$$

where $G_n(s), G_{n-1}(s), \dots, G_1(s)$ *are transfer function matrices of individual sections given by Result 7.*

Proof. It is based on the transfer function representation of the cascade interconnection of n dynamical subsystems given by their transfer functions (see, e.g., Albertos and Sala, 2004). ■

Corollary 8. *Assuming that the observation of the state variables* $x_{1,n}$ *and* $x_{2,n}$ *of the approximation model is made at the end of the cascade (i.e., at* $y_{1,N}$ *and* $y_{2,N}$*) we obtain the following* approximate boundary transfer function *matrix* $\hat{G}(s) = \hat{G}(l_N, s)$*:*

$$\hat{G}(s)=\begin{bmatrix}\hat{g}_{11}(s) & \hat{g}_{12}(s)\\ \hat{g}_{21}(s) & \hat{g}_{22}(s)\end{bmatrix}, \qquad (96)$$

where

$$\hat{g}_{11}(s)=\frac{y_{1,N}(s)}{u_1(s)}, \quad \hat{g}_{12}(s)=\frac{y_{1,N}(s)}{u_2(s)}, \qquad (97)$$

$$\hat{g}_{21}(s)=\frac{y_{2,N}(s)}{u_1(s)}, \quad \hat{g}_{22}(s)=\frac{y_{2,N}(s)}{u_2(s)}, \qquad (98)$$

for zero initial conditions (51) and (52), with $y_{1,N}(s)$*,* $y_{2,N}(s)$ *and* $u_1(s)$*,* $u_2(s)$ *being the Laplace-transformed* N*-th section output (68) and boundary input (67) signals, respectively.*

The transfer function matrix $\hat{G}(s)$ *given by (96)–(98) can be seen as a rational approximation of the irrational boundary transfer function matrix* $G(s)$ *introduced by Corollary 1 and can be obtained as follows:*

$$\hat{G}(s)=G_N(s)G_{N-1}(s)\dots G_1(s), \qquad (99)$$

where $G_N(s), G_{N-1}(s), \dots, G_1(s)$ *are transfer function matrices of individual sections given by Result 7.*

Corollary 9. *From Result 8 we have that the vector of the Laplace-transformed* n*-th section outputs (53) representing approximate state variables* x_1 *and* x_2 *evaluated at* $l = l_n$ *can be calculated as*

$$y_{(n)}(s)=\hat{x}(l_n,s)=\hat{G}(l_n,s)u(s), \qquad (100)$$

with $u(s)$ *being the Laplace transformed boundary input vector (67). Similarly, from Corollary 8 we have that the vector of the Laplace-transformed* N*-th section outputs*

representing approximated output signals y_1 and y_2 can be calculated as

$$y_{(N)}(s) = \hat{y}(s) = \hat{G}(s)u(s). \tag{101}$$

Moreover, by comparing (101) with (75), we obtain

$$\hat{G}(s) = \hat{C}\left(sI - \hat{A}\right)^{-1}\hat{B}, \quad s \in \rho(\hat{A}). \tag{102}$$

representing the well-known transformation from the state-space to the transfer function representation.

Remark 5. As can be seen from (82)–(85) and (99), the degree of the polynomial in the denominators of the elements of the transfer function matrix $\hat{G}(s)$ is equal to $2N$, whereas the degree of the nominators equals N for $\hat{g}_{11}(s)$ and $\hat{g}_{22}(s)$, and $N-1$ for $\hat{g}_{12}(s)$ and $\hat{g}_{21}(s)$. Consequently, the relative degree of $\hat{g}_{11}(s)$ and $\hat{g}_{22}(s)$ is equal to N, and of $\hat{g}_{12}(s)$ and $\hat{g}_{21}(s)$ is equal to $N+1$.

Remark 6. We assume here that in the cascaded system of Fig. 3 no pole-zero cancellation occurs, i.e., the number of poles in $\hat{G}(s)$ is the sum of the number of poles in $G_1(s), G_2(s), \ldots, G_N(s)$, and equals $2N$. In this case, the poles of the approximation model are given by the union of poles of individual sections, and are equal to the eigenvalues (76) of the state-space approximation model. Therefore, in order to ensure the stability of the approximation model $\hat{G}(s)$, all the transfer functions $G_n(s)$, $n = 1, 2, \ldots, N$ need to represent stable dynamical subsystems. This means that the stability condition (64) needs to be fulfilled for each section of the model.

Corollary 10. *The approximation of the constant steady-state solution $\bar{x}(l)$ given by Corollary 3 can be performed, using the approximate distributed transfer function matrix $\hat{G}(l_n, s)$ from Result 8 evaluated at $s = 0$, based on the following equation:*

$$\bar{\hat{x}}(l_n) = \hat{G}(l_n, 0)\bar{u}, \tag{103}$$

where $\bar{u}$ is the constant boundary input vector (42). Consequently, the approximate constant steady-state output vector of the system can be calculated as

$$\bar{\hat{y}} = \hat{G}(0)\bar{u}, \tag{104}$$

where $\hat{G}(0)$ is the approximate boundary transfer function matrix given by Corollary 8, evaluated at $s = 0$.

3.4. Approximation error measures. Here we restrict ourselves to the boundary transfer functions which means that the frequency- and time-domain responses of the original PDE-based model and its MOL-based approximations are to be compared at $l = L$ only. Visual comparison of these responses can be seen as a simple assessment of the quality of the approximation models of different orders. This quality can be expressed in a more accurate, quantitative way using, e.g., the frequency-domain approximation error, defined for the single input–output chanel as

$$e(i\omega) = g(i\omega) - \hat{g}(i\omega), \tag{105}$$

where $g(i\omega)$ is the boundary frequency response of the original infinite-dimensional system and $\hat{g}(i\omega)$ is the boundary frequency response of its finite-dimensional approximation.

Next, an appropriate measure of the approximation error needs to be applied and the two most common metrics used here are the $\mathcal{H}_2$- and $\mathcal{H}_\infty$-norms (Partington, 2004). Assuming that $e(i\omega)$ is strictly proper and has no poles on the imaginary axis, its $\mathcal{H}_2$-norm is finite and given by (Doyle *et al.*, 1992)

$$\|e\,(i\omega)\|_{\mathcal{H}_2} = \sqrt{\frac{1}{2\pi}\int_0^\infty |e\,(i\omega)|^2\,\mathrm{d}\omega}, \tag{106}$$

which, by Parseval's theorem, also represents the square root of the energy of $e(t)$

$$\|e\,(i\omega)\|_{\mathcal{H}_2} = \|e\,(t)\|_{\mathcal{L}_2} = \sqrt{\int_0^\infty |e\,(t)|^2\,\mathrm{d}t}, \tag{107}$$

where

$$e\,(t) = g(t) - \hat{g}(t) \tag{108}$$

is the approximation error of the boundary impulse response.

On the other hand, assuming that $e(i\omega)$ is proper and has no poles on the imaginary axis, its $\mathcal{H}_\infty$-norm is finite and given by

$$\|e\,(i\omega)\|_{\mathcal{H}_\infty} = \sup_\omega |e(i\omega)|\,. \tag{109}$$

For the more general case of a multivariable system, the approximation errors can be written as the matrix

$$E(i\omega) = G(i\omega) - \hat{G}(i\omega), \tag{110}$$

which is 2×2 in our case, and for which the $\mathcal{H}_2$-norm is given by

$$\|E(i\omega)\|_{\mathcal{H}_2} = \sqrt{\frac{1}{2\pi}\int_0^\infty \mathrm{tr}\left[E(-i\omega)^T E(i\omega)\right]\mathrm{d}\omega} \tag{111}$$

and the $\mathcal{H}_\infty$-norm by

$$\|E\,(i\omega)\|_{\mathcal{H}_\infty} = \sup_\omega \bar{\sigma}\,(E(i\omega))\,, \tag{112}$$

where $\bar{\sigma}$ is the maximum singular value of $E(i\omega)$.

As shown by Curtain and Morris (2009), the error in the $\mathcal{H}_\infty$-norm between the original transfer function

$g(s)$ and its approximation $\hat{g}(s)$ yields a uniform bound on the approximation error over all input signals $u(t) \in \mathcal{L}_2$. Transfer functions $g(s) \in \mathcal{H}_\infty$ can be approximated in the $\mathcal{H}_\infty$-norm if they are continuous on the imaginary axis and have a well-defined limit at infinity. A typical example of the system that does not meet these conditions is the pure time-delay system with the irrational transfer function $g(s) = \mathrm{e}^{-\tau s}$. Both the above-mentioned norms are used in the following example to assess the quality of the finite-dimensional approximation models. We restrict ourselves in this example to the two selected input–output channels with different approximation properties.

4. Example: A parallel-flow double-pipe heat exchanger

As an example, we consider here a double-pipe heat exchanger shown in Fig. 4. The mathematical description of its dynamical properties takes, under some simplifying assumptions, the form of the two following PDEs (Zavala-Río *et al.*, 2009; Maidi *et al.*, 2010; Bartecki, 2016):

$$\frac{\partial \vartheta_1(l,t)}{\partial t} + v_1 \frac{\partial \vartheta_1(l,t)}{\partial l} = \alpha_1 \big(\vartheta_2(l,t) - \vartheta_1(l,t)\big), \quad (113)$$

$$\frac{\partial \vartheta_2(l,t)}{\partial t} + v_2 \frac{\partial \vartheta_2(l,t)}{\partial l} = \alpha_2 \big(\vartheta_1(l,t) - \vartheta_2(l,t)\big), \quad (114)$$

where $\vartheta_1(l,t)$ and $\vartheta_2(l,t)$ represent the spatio-temporal temperature distributions of the tube- and shell-side fluids, respectively, t denotes time and $l \in [0, L]$ is the spatial variable with L being the length of the exchanger, v_1 and v_2 represent velocities of the fluids, whereas α_1 and α_2 are generalized parameters including heat transfer coefficients, fluid densities, specific heats, and geometric dimensions of the exchanger. As can be seen, Eqns. (113) and (114) are given in the form of Eqns. (1)–(3) with

$$\Lambda = \begin{bmatrix} v_1 & 0 \\ 0 & v_2 \end{bmatrix}, \quad K = \begin{bmatrix} -\alpha_1 & \alpha_1 \\ \alpha_2 & -\alpha_2 \end{bmatrix}. \quad (115)$$

We consider here the case of the heat exchanger working in the so-called parallel-flow mode, where both fluids flow in the same direction—see solid arrows indicating $v_1 > 0$ and $v_2 > 0$ in Fig. 4. For this configuration we assume the inlet temperatures of both fluids as the input signals,

$$u_1(t) = \vartheta_1(0,t), \quad u_2(t) = \vartheta_2(0,t), \quad (116)$$

which corresponds to the collocated configuration of boundary inputs introduced in (5). The most important, from the control point of view, are the fluid temperatures measured at the exchanger outflow. Therefore, we assume the following output signals:

$$y_1(t) = \vartheta_1(L,t), \quad y_2(t) = \vartheta_2(L,t), \quad (117)$$

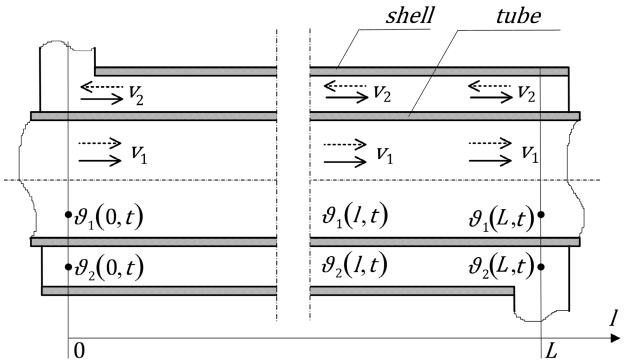

Fig. 4. Cross section along the axis of the double-pipe heat exchanger. Solid arrows show flow directions for the parallel-flow mode and dotted ones—for the counter-flow mode.

which represents the boundary output configuration given by (6). Taking into account the spatio-temporal dynamics of the considered plant, its infinite-dimensional state space representation is given by Result 1 and its distributed and boundary transfer functions are given by Result 2 and Corollary 1, respectively. In the next section we analyze its state-space and transfer function approximation models based on the results presented in Section 3. For this purpose we assume the following parameter values in (113) and (114): $L = 5$ m, $v_1 = 1$ m/s, $v_2 = 0.2$ m/s, $\alpha_1 = \alpha_2 = 0.05$ 1/s.

4.1. Approximate state-space model. Assuming that the heat exchanger model is divided into, e.g., $N = 100$ uniform sections, we obtain the following length of the single section:

$$\Delta l_n = \frac{L}{N} = 0.05 \text{ m}, \qquad n = 1, 2, \ldots, N, \quad (118)$$

and, for the assumed parameter values, the following state-space matrices in (57) and (58):

$$A_n = \begin{bmatrix} -20.05 & 0.05 \\ 0.05 & -4.05 \end{bmatrix}, \quad (119)$$

$$B_n = \begin{bmatrix} 20 & 0 \\ 0 & 4 \end{bmatrix}, \quad C_n = \begin{bmatrix} 1 & 0 \\ 0 & 1 \end{bmatrix}, \quad (120)$$

which after cascade interconnection of N sections yield the state-space approximation model given by Result 6.

4.1.1. Eigenvalues of the approximation model. Since in the considered example we have $\alpha_1 = \alpha_2$ in (115) and, consequently, $k_{12} = k_{21}$ in (3), the state matrix A_n (57) of the single section is real and symmetric (and thus Hermitian) with two real eigenvalues $s_{1,n}$ and $s_{2,n}$. The even partition of the DPS model into $N = 100$

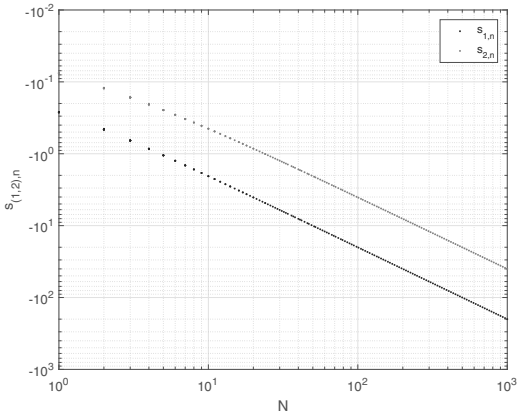

Fig. 5. Logarithmic plot of eigenvalues $s_{(1,2),n}$ of the section state matrix A_n vs. the number of sections N.

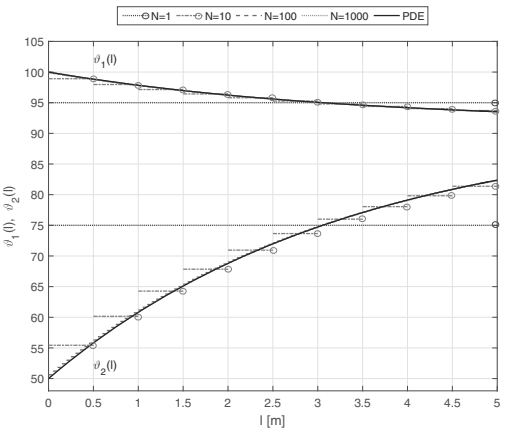

Fig. 6. Constant steady-state temperature profiles $\bar{\vartheta}_1(l)$ and $\bar{\vartheta}_2(l)$ for the PDE and the approximation models (parallel-flow configuration with $\bar{\vartheta}_1(0) = 100°\mathrm{C}$, $\bar{\vartheta}_2(0) = 50°\mathrm{C}$).

sections results in 100 pairs of the following eigenvalues of the approximate state matrix $\hat{A}$ in (71): $s_{1,n} \approx -4.0498$, $s_{2,n} \approx -20.0502$. Since all the eigenvalues are negative, the resulting approximation model is stable, according to Remark 6.

It is obvious that the eigenvalues depend on the value of N. Figure 5 shows the logarithmic plot of $s_{1,n}$ and $s_{2,n}$ vs. the number of (even) sections N. The higher the value of N, the smaller the value of Δl_n in (57) and, consequently, the diagonal elements of A_n become significantly greater than the off-diagonal ones, which results in eigenvalues close to these diagonal terms (see Result 5).

4.1.2. Constant steady-state responses. As was mentioned in Section 2.4, the constant steady-state solution of Eqns. (113)–(117) not only makes it possible to determine the constant outlet temperatures $\bar{\vartheta}_1(L)$ and $\bar{\vartheta}_2(L)$ of the fluids assuming their constant inlet values $\bar{\vartheta}_1(0)$ and $\bar{\vartheta}_2(0)$, but also enables the analysis of their steady-state spatial profiles, $\bar{\vartheta}_1(l)$ and $\bar{\vartheta}_2(l)$ for $l \in [0, L]$, which may be of great importance from a technological point of view.

The steady-state temperature profiles obtained for the considered parallel-flow heat exchanger, both for the original PDE model from Result 3 as well as for the N-section approximation models from Corollary 6, are shown in Fig. 6. As can be seen, the larger the value of N, the better the mapping of the exact steady-state solutions $\bar{\vartheta}_1(l)$ and $\bar{\vartheta}_2(l)$ of the original PDE by their approximations $\bar{\hat{\vartheta}}_1(l)$ and $\bar{\hat{\vartheta}}_2(l)$, respectively.

4.2. Approximate transfer function model. Assuming, in much the same way as in Section 4.1, that the heat exchanger model is evenly partitioned into $N = 100$ sections, we obtain, based on Result 7, the following transfer functions of the single section:

$$g_{11,n}(s) = \frac{20s+81}{p_{A_n}(s)}, \quad g_{12,n}(s) = \frac{0.2}{p_{A_n}(s)}, \tag{121}$$

$$g_{21,n}(s) = \frac{1}{p_{A_n}(s)}, \quad g_{22,n}(s) = \frac{4s+80.2}{p_{A_n}(s)}, \tag{122}$$

with

$$p_{A_n}(s) = s^2 + 24.1s + 81.2 \tag{123}$$

being the characteristic polynomial of the section state matrix A_n in (119).

As stated in Remark 4, the poles of the transfer functions in (121) and (122) are equal to the eigenvalues of A_n and are located at $s_{1,n} \approx -4.0498$ and $s_{2,n} \approx -20.0502$, which means that all considered sections represent stable dynamical subsystems. Therefore, the cascade interconnection of N sections described by the transfer function matrix $G_n(s)$ given by Result 7 leads to the approximation model $\hat{G}(s)$ given by Corollary 8, with N pairs of stable poles $s_{1,n}$ and $s_{2,n}$.

Moreover, the transfer functions $g_{12,n}(s)$ and $g_{21,n}(s)$ in (121) and (122) do not have zeros, whereas $g_{11,n}(s)$ and $g_{22,n}(s)$ have single zeros at $z_{11,n} = -4.05$ and $z_{11,n} = -20.05$, respectively, which means that they represent minimum-phase dynamical subsystems.

4.2.1. Frequency- and time-domain responses. As mentioned in Section 3.4, it is possible, based on the boundary transfer functions $g(s)$ and $\hat{g}(s)$ obtained from the PDE and high-dimensional ODE models, respectively, to compare their dynamical properties, expressed both in the frequency and the time domain. Insights obtained from the frequency and time responses can be useful for the analysis of the impact of the model order on the approximation quality.

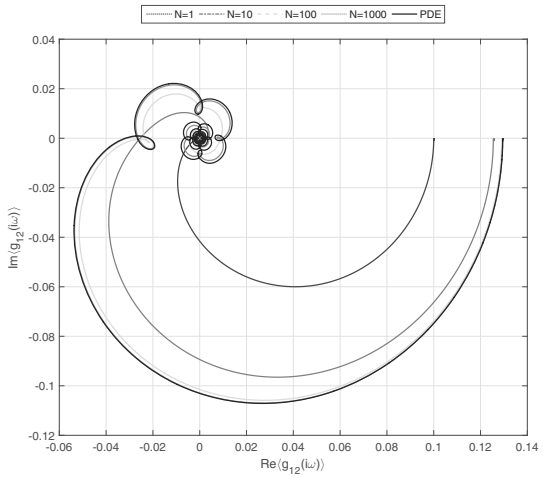

Fig. 7. Nyquist frequency response $g_{12}(s)$ of the PDE model vs. frequency responses $\hat{g}_{12}(s)$ of the approximation models for the parallel-flow heat exchanger.

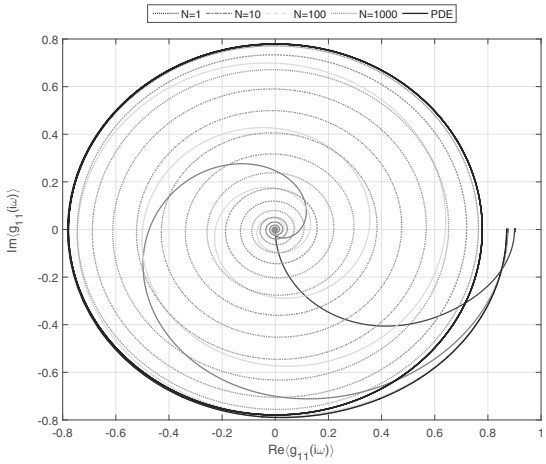

Fig. 9. Nyquist frequency response $g_{11}(s)$ of the PDE model vs. frequency responses $\hat{g}_{11}(s)$ of the approximation models for the parallel-flow heat exchanger.

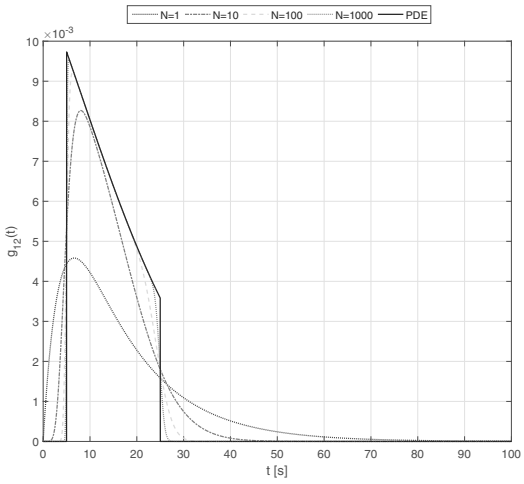

Fig. 8. Impulse response $g_{12}(t)$ of the PDE model vs. impulse responses $\hat{g}_{12}(t)$ of the approximation models for the parallel-flow heat exchanger.

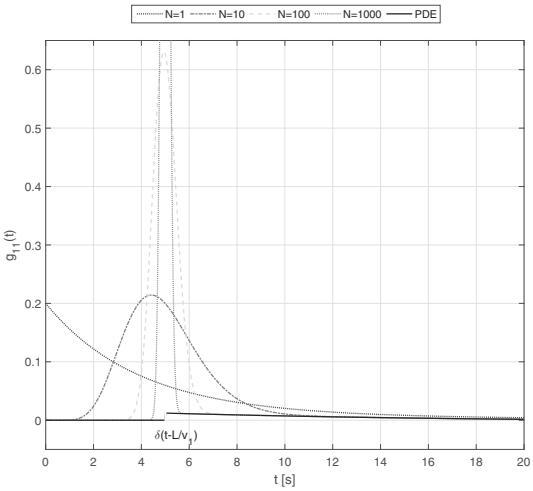

Fig. 10. Impulse response $g_{11}(t)$ of the PDE model vs. impulse responses $\hat{g}_{11}(t)$ of the approximation models for the parallel-flow heat exchanger.

Figure 7 shows the Nyquist plots of the frequency responses for the transfer function channel $g_{12}(s)$ of the considered parallel-flow heat exchanger. It contains both the boundary frequency response $g_{12}(i\omega)$ for the original PDE model and the responses $\hat{g}_{12}(i\omega)$ of its rational approximations with different numbers N of sections. One can observe characteristic "loops" on the Nyquist plot which are associated with the resonance-like phenomena taking place inside the heat exchanger. Such dynamical behavior is reported in the literature on heat exchangers as well as it is known from the real-plant experiments (Bartecki, 2015b; Lalot and Desmet, 2019). As in the case of the previously analyzed constant steady-state responses, it can be stated that the larger the order of the approximation model, the better the mapping of the original frequency response, together with the above-mentioned oscillations.

Similar conclusions can be drawn based on the analysis of boundary the impulse responses $g_{12}(t)$ for the same input–output channel (Fig. 8). In order to correctly map the fairly steep slopes of the original impulse response of the PDE model, a relatively high order ODE-based model is needed which is able to correctly approximate its high-frequency modes.

The analogous plots for the transfer function channel $g_{11}(s)$ are presented in Figs. 9 and 10. As can be seen

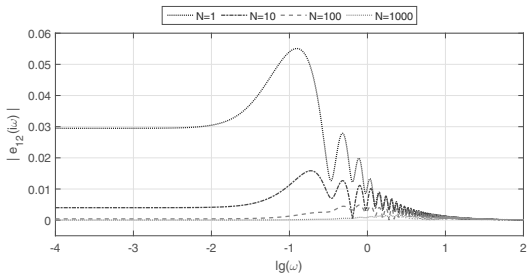

Fig. 11. Approximation error magnitudes $|e_{12}(i\omega)|$ for different numbers of sections N.

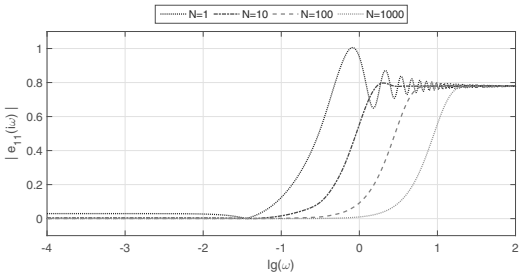

Fig. 12. Approximation error magnitudes $|e_{11}(i\omega)|$ for different numbers of sections N.

Table 1. Boundary magnitude values and norm estimates of $e_{12}(i\omega)$ for $\omega \in [10^{-4}, 10^2]$.

N	$\lvert e_{12}\rvert_{\omega=10^{-4}}$	$\lvert e_{12}\rvert_{\omega=10^2}$	$\lVert e_{12}\rVert_{\mathcal{H}_2}$	$\lVert e_{12}\rVert_{\mathcal{H}_\infty}, \omega_p$
1	$2.95\cdot10^{-2}$	$1.15\cdot10^{-4}$	1.11	$5.51\cdot10^{-2}$, 0.12
10	$4.01\cdot10^{-3}$	$1.15\cdot10^{-4}$	0.24	$1.59\cdot10^{-2}$, 0.19
100	$4.16\cdot10^{-4}$	$1.15\cdot10^{-4}$	0.07	$4.85\cdot10^{-3}$, 0.79
1000	$4.18\cdot10^{-5}$	$1.15\cdot10^{-4}$	0.02	$1.53\cdot10^{-3}$, 2.36

Table 2. Boundary magnitude values and norm estimates of $e_{11}(i\omega)$ for $\omega \in [10^{-4}, 10^2]$.

N	$\lvert e_{11}\rvert_{\omega=10^{-4}}$	$\lvert e_{11}\rvert_{\omega=10^2}$	$\lVert e_{11}\rVert_{\mathcal{H}_2}$	$\lVert e_{11}\rVert_{\mathcal{H}_\infty}, \omega_p$
1	$2.95\cdot10^{-2}$	0.78	20.80	1.00, 0.82
10	$4.01\cdot10^{-3}$	0.78	18.11	0.80, 2.03
100	$4.16\cdot10^{-4}$	0.78	15.66	0.78, 7.97
1000	$4.18\cdot10^{-5}$	0.78	12.83	0.78, 34.08

here, the approximation models of increasing orders try to fit the responses of the infinite-dimensional system. However, due to the dominating time-delay nature of this channel, which results in the original frequency response having no limit at infinity (see Fig. 9) and the impulse response containing Dirac's delta distribution at $t = L/v_1 = 5$ s (see Fig. 10), the approximation task is definitely more difficult here than in the previous case.

4.2.2. Approximation error analysis. The analysis below is based on the considerations presented in Section 3.4. Figures 11 and 12 shows the magnitude plots of the approximation errors $e_{12}(i\omega)$ and $e_{11}(i\omega)$, respectively, obtained for different N based on (105). More detailed data concerning the error magnitude and $\mathcal{H}_2$- and $\mathcal{H}_\infty$-norm values given by (106) and (109), respectively, estimated numerically for $\omega \in [10^{-4}, 10^2]$ are presented in Table 1 for $e_{12}(i\omega)$ and in Table 2 for $e_{11}(i\omega)$. At first glance, it is evident that for $g_{12}(s)$ the approximation is better for higher frequencies than for lower ones, whereas for $g_{11}(s)$ the opposite is true. More specifically, it can be stated that for the case of the "crossover" transfer function channel $g_{12}(s)$, the magnitude of the approximation error tends to zero as the frequency tends to infinity, and its maximal value decreases as the number of sections N increases (Fig. 11). Consequently, both approximation norms, $\|e_{12}(i\omega)\|_{\mathcal{H}_2}$ given by (106) and $\|e_{12}(i\omega)\|_{\mathcal{H}_\infty}$ given by (109) seem to tend to zero as N goes to infinity.

In contrast, for the "straightforward" transfer function channel $g_{11}(s)$, the magnitude of the approximation error stabilizes, with increasing frequency, to a non-zero constant level which does not depend on N (Fig. 12). Consequently, its $\mathcal{H}_2$-norm is infinite and its $\mathcal{H}_\infty$-norm does not decrease as N increases. The results for the transfer function channels $g_{21}(s)$ and $g_{22}(s)$, which are not shown here due to limited space, were similar, in qualitative terms, to the ones obtained for $g_{12}(s)$ and $g_{11}(s)$, respectively.

To sum up, the MOL-based approximation of the "straightforward" transfer function channels $g_{11}(s)$ and $g_{22}(s)$ produces significantly worse results than approximation of the "crossover" channels $g_{12}(s)$ and $g_{21}(s)$. The main reason is the time-delay nature of the first two transfer functions, for which, as is well known, the rational approximation makes sense only over a finite frequency band. It should be noted that for both types of input–output channels, increasing the number of sections of the approximation model contributes to the increase in the model accuracy in the low and medium frequency ranges.

5. Summary

In this paper we have discussed some results concerning finite-dimensional approximation of DPSs described by linear hyperbolic equations with boundary conditions representing collocated external inputs to the system. The approximation model has been considered here in the form of a cascade interconnection of a number of sections expressed both in the state-space and the transfer function domains, resulting in a high-order, finite-dimensional model. The quality of such models of different orders has been verified by comparing their boundary frequency-

and time-domain responses and measured using $\mathcal{H}_2$- and $\mathcal{H}_\infty$-norms of the approximation error.

It has been shown here that for the same DPS there may exist transfer functions with different approximation properties which depend on the boundary conditions. Referring to the specific case considered in the paper, all the irrational transfer functions of the original 2×2 hyperbolic system have the same denominators, since they are based on the same resolvent of the state space operator A. However, they differ in their numerators which largely depend on the boundary input–output configuration. Consequently, for the "crossover" input–output channels the in-domain effects prevail which are easier to approximate using rational transfer functions, whereas for the "straightforward" channels the time-delay phenomena dominate which make the approximation task more difficult.

The obtained approximate state-space and transfer function models can be used to accomplish controller design for the 2×2 hyperbolic systems, using conventional control schemes, without recourse to complex DPS theory. However, the main drawback of the presented approach is that the resulting approximation models can be of a very high order—even in thousands, as presented in the paper. Therefore, the next step to be performed is to obtain a lower-order model, using, e.g., a balancing realization approach. Another option is to use a different approximation approach than the MOL strategy presented here, e.g., one of the techniques which have been found effective in the model reduction of time-delay systems. These include, i.a., Fourier–Laguerre series, Padé approximants, shift-based approximations, Malmquist bases, partial fractions, wavelet-based techniques, Hankel-norm approximants and truncated state-space realizations (see Partington, 2004).

Another task to be performed is to develop similar approximate state-space and transfer function models for the *anti-collocated* boundary input configuration, occurring, e.g., in counter-flow heat exchangers. An even more general approach could consist in a generalization of the presented results to $n \times m$ hyperbolic systems, i.e., systems with n equations convecting in one direction and m equations convecting in the opposite direction, as considered by Hu *et al.* (2016) and Anfinsen *et al.* (2017).

References

Ahmad, I. and Berzins, M. (2001). MOL solvers for hyperbolic PDEs with source terms, *Mathematics and Computers in Simulation* **56**(2): 115–125.

Albertos, P. and Sala, A. (2004). *Multivariable Control Systems: An Engineering Approach*, Springer, London.

Anfinsen, H. and Aamo, O.M. (2018). Adaptive control of linear 2×2 hyperbolic systems, *Automatica* **87**: 69–82.

Anfinsen, H. and Aamo, O.M. (2019). *Adaptive Control of Hyperbolic PDEs*, Springer, Cham.

Anfinsen, H., Diagne, M., Aamo, O. and Krstić, M. (2017). Estimation of boundary parameters in general heterodirectional linear hyperbolic systems, *Automatica* **79**: 185–197.

Arov, D.Z., Kurula, M. and Staffans, O.J. (2012). Boundary control state/signal systems and boundary triplets, *in* A. Hassi *et al.* (Eds), *Operator Methods for Boundary Value Problems*, Cambridge University Press, Cambridge, pp. 73–86.

Bartecki, K. (2013a). Computation of transfer function matrices for 2×2 strongly coupled hyperbolic systems of balance laws, *Proceedings of the 2nd Conference on Control and Fault-Tolerant Systems, Nice, France*, pp. 578–583.

Bartecki, K. (2013b). A general transfer function representation for a class of hyperbolic distributed parameter systems, *International Journal of Applied Mathematics and Computer Science* **23**(2): 291–307, DOI: 10.2478/amcs-2013-0022.

Bartecki, K. (2015a). Abstract state-space models for a class of linear hyperbolic systems of balance laws, *Reports on Mathematical Physics* **76**(3): 339–358.

Bartecki, K. (2015b). Transfer function-based analysis of the frequency-domain properties of a double pipe heat exchanger, *Heat and Mass Transfer* **51**(2): 277–287.

Bartecki, K. (2016). *Modeling and Analysis of Linear Hyperbolic Systems of Balance Laws*, Springer, Cham.

Bartecki, K. (2019). Approximation state-space model for 2×2 hyperbolic systems with collocated boundary inputs, *24th International Conference on Methods and Models in Automation and Robotics (MMAR), Międzyzdroje, Poland*, pp. 513–518.

Bastin, G. and Coron, J.-M. (2016). *Stability and Boundary Stabilization of 1-D Hyperbolic Systems*, Birkhäuser, Basel.

Callier, F.M. and Winkin, J. (1993). Infinite dimensional system transfer functions, *in* R.F. Curtain *et al.* (Eds), *Analysis and Optimization of Systems: State and Frequency Domain Approaches for Infinite-Dimensional Systems*, Springer, Berlin/Heidelberg, pp. 75–101.

Cockburn, B., Johnson, C., Shu, C. and Tadmor, E. (1998). *Advanced Numerical Approximation of Nonlinear Hyperbolic Equations*, Springer, Heidelberg.

Coron, J., Li, T. and Li, Y. (2019). *One-Dimensional Hyperbolic Conservation Laws and Their Applications*, World Scientific, Singapore.

Curtain, R.F. and Zwart, H. (1995). *An Introduction to Infinite-Dimensional Linear Systems Theory*, Springer, New York, NY.

Curtain, R. and Morris, K. (2009). Transfer functions of distributed parameters systems: A tutorial, *Automatica* **45**(5): 1101–1116.

Deutscher, J. (2017). Finite-time output regulation for linear 2×2 hyperbolic systems using backstepping, *Automatica* **75**: 54–62.

Doyle, J., Francis, B. and Tannenbaum, A. (1992). *Feedback Control Theory*, Macmillan, New York, NY.

Emirsajłow, Z. and Townley, S. (2000). From PDEs with boundary control to the abstract state equation with an unbounded input operator: A tutorial, *European Journal of Control* **6**(1): 27–49.

Engel, K.-J. and Nagel, R. (2000). *One-Parameter Semigroups for Linear Evolution Equations*, Springer, New York, NY.

Godlewski, E. and Raviart, P.-A. (1996). *Numerical Approximation of Hyperbolic Systems of Conservation Laws*, Springer, New York, NY.

Grabowski, P. and Callier, F.M. (2001). Circle criterion and boundary control systems in factor form: Input–output approach, *International Journal of Applied Mathematics and Computer Science* **11**(6): 1387–1403.

Gugat, M., Herty, M. and Yu, H. (2018). On the relaxation approximation for 2×2 hyperbolic balance laws, *in* C. Klingenberg and M. Westdickenberg (Eds), *Theory, Numerics and Applications of Hyperbolic Problems I*, Springer, Cham, pp. 651–663.

Hu, L., Di Meglio, F., Vazquez, R. and Krstić, M. (2016). Control of homodirectional and general heterodirectional linear coupled hyperbolic PDEs, *IEEE Transactions on Automatic Control* **61**(11): 3301–3314.

Jones, B.L. and Kerrigan, E.C. (2010). When is the discretization of a spatially distributed system good enough for control?, *Automatica* **46**(9): 1462–1468.

Kitsos, C., Besançon, G. and Prieur, C. (2019). A high-gain observer for a class of 2×2 hyperbolic systems with C1 exponential convergence, *IFAC-PapersOnLine* **52**(2): 174–179.

Koto, T. (2004). Method of lines approximations of delay differential equations, *Computers & Mathematics with Applications* **48**(1–2): 45–59.

Lalot, S. and Desmet, B. (2019). The harmonic response of counter-flow heat exchangers—Analytical approach and comparison with experiments, *International Journal of Thermal Sciences* **135**: 163–172.

LeVeque, R. (2002). *Finite Volume Methods for Hyperbolic Problems*, Cambridge University Press, Cambridge.

Levine, W.S. (Ed.) (2011). *The Control Systems Handbook: Control System Advanced Methods*, Electrical Engineering Handbook, CRC Press, Boca Raton, FL.

Li, H.-X. and Qi, C. (2010). Modeling of distributed parameter systems for applications—A synthesized review from time-space separation, *Journal of Process Control* **20**(8): 891–901.

Litrico, X. and Fromion, V. (2009a). Boundary control of hyperbolic conservation laws using a frequency domain approach, *Automatica* **45**(3): 647–656.

Litrico, X. and Fromion, V. (2009b). *Modeling and Control of Hydrosystems*, Springer, London.

Maidi, A., Diaf, M. and Corriou, J.-P. (2010). Boundary control of a parallel-flow heat exchanger by input–output linearization, *Journal of Process Control* **20**(10): 1161–1174.

Mattheij, R.M.M., Rienstra, S.W. and ten Thije Boonkkamp, J.H.M. (2005). *Partial Differential Equations: Modeling, Analysis, Computation*, SIAM, Philadelphia, PA.

Partington, J.R. (2004). Some frequency-domain approaches to the model reduction of delay systems, *Annual Reviews in Control* **28**(1): 65–73.

Polyanin, A.D. and Manzhirov, A.V. (1998). *Handbook of Integral Equations*, CRC Press, Boca Raton, FL.

Rauh, A., Senkel, L., Aschemann, H., Saurin, V.V. and Kostin, G.V. (2016). An integrodifferential approach to modeling, control, state estimation and optimization for heat transfer systems, *International Journal of Applied Mathematics and Computer Science* **26**(1): 15–30, DOI: 10.1515/amcs-2016-0002.

Ray, W.H. (1981). *Advanced Process Control*, McGraw-Hill New York, NY.

Russell, D.L. (1978). Controllability and stabilizability theory for linear partial differential equations: Recent progress and open questions, *SIAM Review* **20**(4): 639–739.

Schiesser, W.E. and Griffiths, G.W. (2009). *A Compendium of Partial Differential Equation Models: Method of Lines Analysis with Matlab*, Cambridge University Press, New York, NY.

Shakeri, F. and Dehghan, M. (2008). The method of lines for solution of the one-dimensional wave equation subject to an integral conservation condition, *Computers & Mathematics with Applications* **56**(9): 2175–2188.

Tucsnak, M. and Weiss, G. (2009). *Observation and Control for Operator Semigroups*, Birkhäuser, Basel.

Zavala-Río, A., Astorga-Zaragoza, C.M. and Hernández-González, O. (2009). Bounded positive control for double-pipe heat exchangers, *Control Engineering Practice* **17**(1): 136–145.

Zwart, H. (2004). Transfer functions for infinite-dimensional systems, *Systems and Control Letters* **52**(3–4): 247–255.

Krzysztof Bartecki received an MSc and a PhD in electrical engineering, as well as a DSc in automatic control and robotics from the Faculty of Electrical, Control and Computer Engineering, Opole University of Technology, in 1996, 2004 and 2016, respectively. Since 2017, he has been an associate professor at the Institute of Control Engineering there. He has authored or coauthored about 60 papers, mainly on mathematical modeling of distributed parameter systems.

Received: 12 February 2020
Revised: 28 April 2020
Accepted: 29 May 2020